Korean J. Chem. Eng., 40(11), 2602-2611 (2023)
DOI: 10.1007/s11814-023-1524-x

pISSN: 0256-1115
eISSN: 1975-7220

Determining adsorbent performance degradation in pressure swing adsorption using a deep learning algorithm and one-dimensional simulator

Seongmin Son[*,**,†]

*Department of Smart Plant Engineering, Kyungpook National University, Sangju 37224, South Korea
**Department of Convergence & Fusion System Engineering, Kyungpook National University, Sangju 37224, South Korea
(*Received 30 March 2023 • Revised 28 May 2023 • Accepted 29 June 2023*)

Abstract−This study proposes a methodology for diagnosing the degree of performance degradation of the adsorbent in pressure swing adsorption (PSA) plants using a one-dimensional simulator and a time-series deep learning algorithm. First, a 1D PSA simulator was developed using mathematical models and validated with previously published experimental data. The behavior change of the PSA plant according to the performance degradation was trained using a deep learning algorithm based on the developed simulator. The model combines the 1D convolutional neural network and long-short-term memory (LSTM) network. The prediction of the degradation degree of the internal adsorbent was then presented using a pretrained neural network. The developed methodology demonstrates a mean squared error lower than 10^{-6} when predicting the degree of adsorbent degradation from the adsorption-bed-temperature time-series profiles with an example. The methodology can be used to predictive maintenance strategy by identifying PSA performance degradation in real time without stopping operation.

Keywords: Pressure Swing Adsorption, Degradation, Abnormal Detection, Simulation

INTRODUCTION

The pressure swing adsorption (PSA) process is a widely known gas-gas separation technique that exploits the different adsorption characteristics of the adsorbents and gas species in a mixture [1]. This process typically involves multiple adsorption beds to separate products with the desired purity from the feed gas through adsorption at high pressures, followed by desorption using a suitable purge gas at low pressures.

During the adsorption process, the different adsorption forces of each gas molecule cause different movement speeds of the gases on the adsorption bed. Based on these speed differences, gas species can be purified or separated from the mixture using the same principle as that employed in chromatography.

Typically, adsorption capacity is proportional to the pressure [2,3] and adsorbents can regain their adsorption capacity during the desorption process at low pressures. PSA is a cyclical adsorption-desorption process carefully designed to provide a continuous supply of product gas with the desired purity.

With the increasing importance of low-carbon processes to mitigate climate change, the PSA process has been attracting renewed attention for hydrogen separation and purification [4] and carbon capture [5]. Recent PSA-related studies have focused mainly on improving the separation performance using model-based design approaches [6-8]. To achieve this goal, one-dimensional (1D) mathematical models for PSA systems and their suitable boundary conditions for each process step are actively being studied [1]. Through this methodology, optimization studies for PSA processes are being conducted using traditional algorithms [9] or deep learning models [10].

PSA plants are usually designed with a guaranteed lifetime of >10 years [11], and replacement of adsorbents is generally not considered during the design stage. However, this design criterion can sometimes lead to severe problems. For instance, adsorbents can be damaged because of highly concentrated water resulting from the feed gas containing an excessive amount of moisture compared that considered in the design process. This can substantially reduce the performance of adsorbents such as zeolites, which are known to undergo structural damage under high vapor pressures [12]. Moreover, if a feed gas containing impurities not considered in the design stage is provided, long-term performance degradation of the adsorbents may occur. For example, when purifying hydrogen using coke oven gas, the gas may contain various impurities, such as dust, oil, tar, BTXs, and C3+ [13], which are usually not considered in the process-design study [14].

Although it is difficult to consider all such impurities in the design stage for various reasons, the adsorbent performance can deteriorate gradually over time because of various mechanisms, such as blocking of adsorption pores, reduction in the surface area, and mechanical destruction of adsorbent particles. However, from the operation and maintenance viewpoint, studies on PSA have not been conducted extensively. Most aging or performance degradation analyses of the adsorption process have mainly focused on the deterioration of the adsorbent itself [15, 16]. Therefore, from a process perspective, further research is required to study the effect of adsorbent degradation or predict the degree of adsorbent aging.

A methodology for diagnosing the degree of performance deterioration of an adsorbent is proposed in this study using a 1D PSA process model and a time-series deep learning algorithm. First, a

†To whom correspondence should be addressed.
E-mail: seongminson@knu.ac.kr

database is built on performance deterioration using the developed PSA simulator. Based on the database, a pretrained network is developed using supervised learning and a method of inversely estimating the degree of performance degradation of the PSA internal adsorbent is presented. To validate the performance of the methodology, a virtual example case is given. The main objective of the methodology is to find the simplified-linear-degradation factor of a given adsorbent through measurements that can easily be done in real time. Temperature profiles on the wall or inside the bed are good candidates for this purpose. These datasets are dynamically behaved over time and are closely influenced by the adsorption and desorption phases, and as the amount of adsorption/desorption changes due to the degradation of the adsorbent, the total heat of adsorption/desorption also changes, which is a factor that is directly affected by the degree of degradation. For these reasons, temperature profiles of a single PSA bed are selected for the example case of this diagnosis algorithm.

DEVELOPMENT OF THE PSA SIMULATOR

1. Governing Equations for the PSA System

Fully dynamic adsorption processes are involved in PSA; therefore, it is necessary to construct time-dependent differential equations to model it. The PSA simulator was developed using the following equations, as stated in many of the previous modeling studies [17]:

- Overall mass balance for an ideal gas [18,19]

$$-D_L\frac{\partial^2 P}{\partial z^2}+u\frac{\partial P}{\partial z}+P\frac{\partial u}{\partial z}+\frac{\partial P}{\partial t}+PT\left(-D_L\frac{\partial^2}{\partial z^2}\left(\frac{1}{T}\right)+\frac{\partial}{\partial t}\left(\frac{1}{T}\right)+u\frac{\partial}{\partial z}\left(\frac{1}{T}\right)\right)$$
$$-2D_L\frac{\partial}{\partial Z}\left(\frac{1}{T}\right)\frac{\partial P}{\partial z}+\rho_p RT\left(\frac{1-\varepsilon}{\varepsilon}\right)\Sigma\frac{\partial \bar{q}_i}{\partial t}=0. \quad (1)$$

- Species mass balance for an ideal gas [18,19]

$$-D_L\frac{\partial^2 y_i}{\partial z^2}+u\frac{\partial y_i}{\partial z}+\frac{\partial y_i}{\partial t}+\rho_p\frac{RT}{P}\left(\frac{1-\varepsilon}{\varepsilon}\right)\frac{\partial \bar{q}_i}{\partial t}=0. \quad (2)$$

- Energy balance in the adsorption column [20,21]

$$-K_L\frac{\partial^2 T}{\partial z^2}+\varepsilon\rho_g C_{pg}\left(u\frac{\partial T}{\partial z}+T\frac{\partial u}{\partial z}\right)+(\varepsilon_t\rho_g C_{pg}+\rho_B C_{ps})\frac{\partial T}{\partial t}$$
$$-\rho_B\left(\Sigma\Delta_i\frac{\partial \bar{q}_i}{\partial t}\right)+\frac{2h_i}{R_{Bi}}(T-T_w)=0. \quad (3)$$

- Heat loss through a wall to ambient [17]

$$\rho_W C_{pw}A_w\frac{\partial T_w}{\partial t}-2\pi R_{Bi}h_i(T-T_w)+2\pi R_{Bo}h_o(T_w-T_{amb})=0. \quad (4)$$

- Momentum conservation (Ergun's Eq. [20])

$$-\frac{dP}{dz}=\frac{150(1-\varepsilon)^2}{4R_p^2\varepsilon}\mu u+1.75\frac{1-\varepsilon}{2R_p\varepsilon}\rho\,\mu\,u|u| \quad (5)$$

- Extended Langmuir Isotherm

$$q_i^*=\frac{(a_{i0}+a_{i1}T)\left(b_{i0}\exp\left(\frac{b_{i1}}{T}\right)\right)P_i}{1+\Sigma_j b_{j0}\exp\left(\frac{b_{j1}}{T}\right)P_j} \quad (6)$$

This set of governing equations is based on the following assumptions [17]:

1. Ideal gas law
2. The flow patterns of gas inside the adsorption beds follow an axially-dispersed plug-flow model
3. The adsorption rate can be described by the linear driving force (LDF) model [21]
4. Adsorption beds are of the packed type and have uniform voidage
5. 1D and no radial property distributions (such as temperatures, pressures, and concentrations)
6. Cylindrical adsorption-bed geometry

Additionally, beyond the breakthrough analysis, more assumptions for pressure-changing steps, such as blowdown, pressurization, and equalization process, are adopted. These additional assumptions are as follows [18,22]:

7. The pressure drops inside the adsorption bed during the pressure-changing steps are negligible
8. The pressure-changing ratio is linear during the pressure-changing steps
9. Velocity profiles during the pressure-changing steps are linear

Finally, to model the performance degradation of adsorbents inside the PSA plant, it is necessary to define adsorption isotherm models while considering the adsorbent degradation. It is generally known that this part can be represented in the form of a linear equation. Therefore, in this study, a linear performance degradation model is assumed for an analysis [23,24]. This empirical model uses a simple multiplication factor k to model the degree of adsorbent degradation, as shown in Eq. (7):

$$q^*_{degraded}=k_d q^*_{fresh}. \quad (7)$$

Under this assumption, this research was conducted using a software developed in-house. The code was developed based on Python v3.7 [25]. The simulator developed according to the above equations was written to calculate the cyclic steady state of the PSA process through iterative computation. The convergence of the calculation was judged by whether the stepwise errors of both purity and recovery were within 0.05%.

2. Validation of the Developed Code System

The developed simulator was verified using experimental data. The target experiment was a breakthrough experiment by Ahn et al. [26], which was used to validate the developed simulator. A breakthrough experiment determines the adsorption characteristics of an adsorbent inside a column by injecting a mixture of gases of a known composition into the column and then measuring the change in the composition at the outlet. Usually, the experiment is performed until the composition of a given feed gas and the column exit composition become identical. The moment when the adsorbent no longer adsorbs a particular species and that species is observed at the column exit is called the breakthrough. Ahn's experiment [24] was based on a 60.4 : 28.1 : 11.5 vol% hydrogen ternary mixture of $H_2/CH_4/CO$ on a Cargon activated carbon column. The outlet composition, temperature evolution, and temperature distribution as functions of time are provided in the reference [26].

To validate the model with the experiment, model parameters and adsorption characteristics are needed. Table 1 shows the char-

Table 1. Characteristics of the activated carbon and adsorption-bed information [26]

Item	Unit	Value
Average pellet size (R_p)	m	1.15×10^{-3}
Pellet density (ρ_p)	kg/m^3	850
Bulk density (ρ_B)	kg/m^3	482
Bed porosity (ε_B)	-	0.433
Total void porosity (ε_t)	-	0.780
Pellet heat capacity (ε)	J/kg/K	1046
Axial thermal diffusivity (K_L)	J/m/sec/K	0.406
Wall density (ρ_w)	kg/m^3	7830
Wall heat capacity (C_{pw})	J/kg/K	523
Internal heat transfer coefficient (h_i)	J/m^2/sec/K	87.864
External heat transfer coefficient (h_o)	J/m^2/sec/K	225.936
Bed length (L)	m	1
Bed inner radius (R_{Bi})	m	0.0371
Bed outer radius (R_{Bo})	m	0.0452

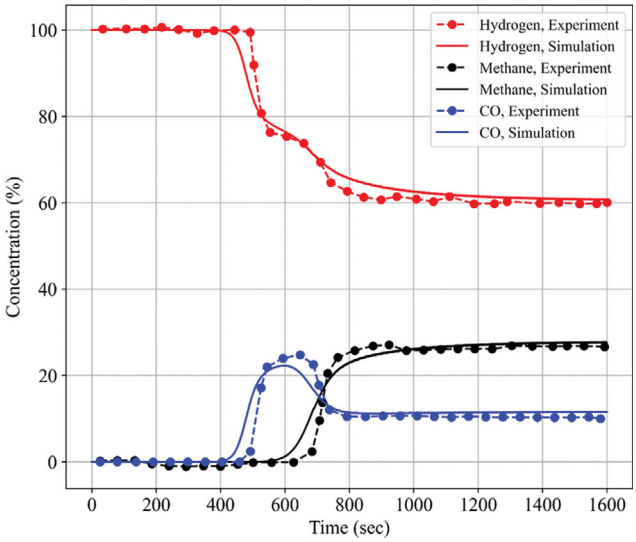

Fig. 1. Breakthrough curves of the ternary mixture (H_2/CH_4/CO) in the activated carbon bed.

acteristics of the adsorbent (activated carbon) and adsorption-bed information [26].

The adsorption isotherm model is utilized as the extended Langmuir adsorption isotherm, and the parameters are from the literature [27]. The isotherm model is shown in Eq. (6); parameters are shown in Table 2.

This information is inserted into the simulator to validate the code by comparing it with experiments. The objects of the comparison are as follows: (1) the outlet composition over time and (2) the temperature distribution in the adsorption bed over time. Fig. 1 shows the breakthrough curve between the developed simulator's results and experimental values. Fig. 2 shows the comparison of the temperature distribution in the adsorption bed over time between the experiment and simulation. As presented in the figures, the developed simulator analyzes the dynamics of the given adsorption col-

Table 2. Langmuir parameters, LDF coefficients, and isosteric heats of adsorption of the activated carbon [27]

			H_2	CO	CH_4	CO_2	N_2
Langmuir parameters	a_0	mol/kg	16.943	33.85	23.86	22.7973	1.6441
	a_1	mol/K/kg	−0.021	−0.09072	−0.05621	−0.07	−0.00073
	b_0	1/bar	6.248E-5	2.311E-4	3.478E-3	0.01	0.0545
	b_1	K	1229	1751	1159	1030	326
LDF coefficient	k	1/s	0.7	0.15	0.195	0.0355	0.261
Heat of adsorption	ΔH	cal/mol	2880	4300	4290	5240	1660

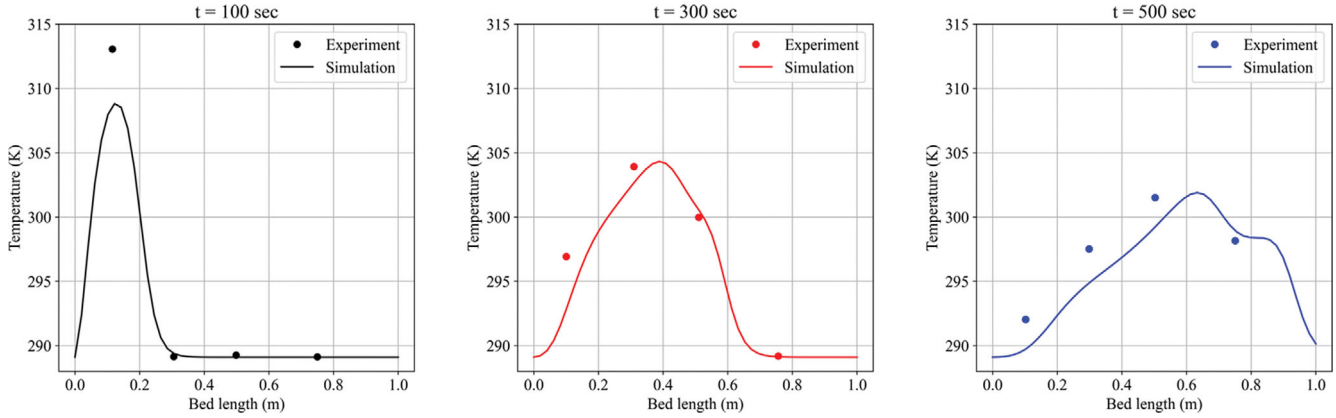

Fig. 2. Comparison of temperature distributions in the adsorption bed over time between the experiment and simulation (adsorption time=100, 300, and 500 s).

umn well.

EXAMPLE CASE: STEAM-METHANE REFORMING PSA

Steam-methane reforming (SMR) is a typical process for producing hydrogen from fossil fuels, in which natural gas (methane) and water react at high temperatures to produce hydrogen and CO_2. Currently, hydrogen is mostly produced using this process [28]; the equation for this chemical reaction is as follows:

$$CH_4+2H_2O \rightarrow 4H_2+CO_2.$$

Ideally, in the SMR process, one molecule of methane reacts with two molecules of water under catalytic conditions to produce one molecule of carbon dioxide and three molecules of hydrogen. The resulting H_2-rich mix gas is usually separated and purified via PSA. The adsorbents employed in PSA plants are typically activated carbon, zeolites (zeolite 4A, 5A, etc.), or a combination of both [28].

As the focus of this study is not on the design of the carbon capture process but on the real-time adsorbent-degradation diagnosis algorithm using a suitable deep learning algorithm, it is assumed that the process is performed through the sole activated carbon adsorption bed. This is verified by a comparison with experiments in Section 2.2, confirming the consistency between the analytical and experimental results. Moreover, in practice, various impurities (such as dust, unreacted methane, and nitrogen) might be generated during the SMR process. In this study, it is assumed that the feed gas reacted ideally and had an $H_2:CO_2$ ratio of 4:1 for the same purpose.

1. Conditions for Simulation of the PSA System

For the example PSA plant, a four-bed eight-step PSA sequence is considered [29] (Fig. 3).

Fig. 4 shows the isotherms of CO_2 and H_2 calculated by using the extended Langmuir model at room temperature (298 K). As can be seen, the adsorbent used in this example has a superior ability for adsorbing CO_2 compared to adsorbing H_2. Taking this into account, it is assumed that the activated carbon would not adsorb any H_2 when creating the database. Therefore, the degradation factor

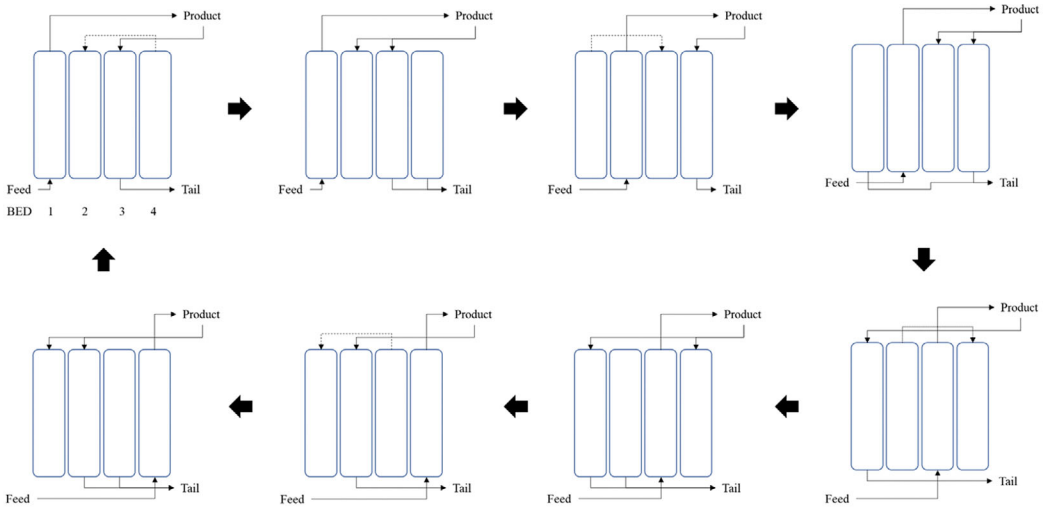

Time	t1	t2	t1	t2	t1	t2	t1	t2
SEQ#	1	2	3	4	5	6	7	8
BED1	ADS		DEQ	BD	PG		PEQ	PR
BED2	PEQ	PR	ADS		DEQ	BD	PG	
BED3	PG		PEQ	PR	ADS		DEQ	BD
BED4	DEQ	BD	PG		PEQ	PR	ADS	

STEP	ADS	PG	PR	BD	PEQ	DEQ
Boundary Condition	Given: $u(z=0)$, $P(z=0)$, $T(z=0)$, $yi(z=0)$	Given: $u(z=L)$, $P(z=L)$ $T(z=L)$, $yi(z=L)$	Given: $P(z=L$ over time$)^*$ $T(z=L)$, $yi(z=L)$	Given: $P(z=0$ over time$)^*$ $T(z=0)$, $yi(z=0)$	$P_{PEQ}(z=L)^* = P_{DEQ}(z=L)^*$ $A_{PEQ}u_{PEQ}(z=L)=A_{DEQ}u_{DEQ}(z=L)$ $T_{PEQ}(Z=L)=T_{DEQ}(z=L)$ $yi_{PEQ}(z=L)=yi_{DEQ}(z=L)$	

(*Calculate via linear pressure change approach)

Fig. 3. Four-bed eight-step PSA sequence of the example study and boundary conditions for each step (ADS, adsorption step; BD, blowdown step; DEQ, depressurizing pressure-equalization step; PEQ, pressurizing pressure-equalization step; PR, pressurization step; and PG, purge step).

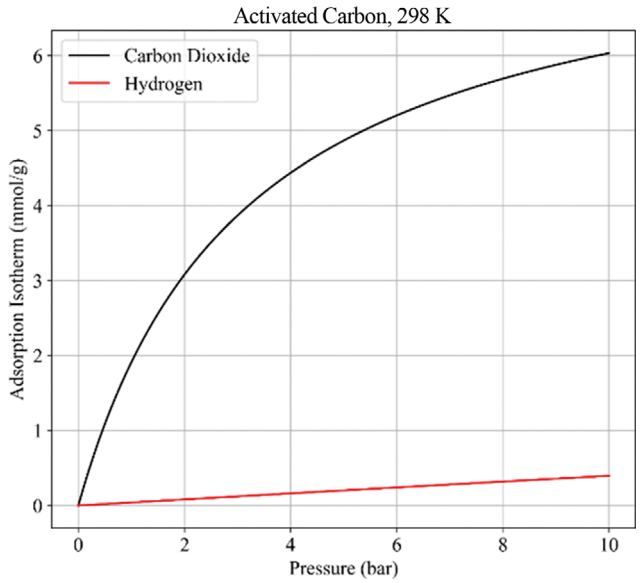

Fig. 4. Adsorption isotherms of CO_2 and H_2 predicted using the extended Langmuir model.

(k_d) for hydrogen in the adsorbent is not considered in this example problem.

The geometric information on the adsorption beds is presented in Table 1. Adsorbent inside the PSA plant is assumed to be the activated carbon. The kinetics and isotherm of the adsorbent used are the same as in Table 2. Other assumed plant parameters of the process are shown in Table 3. These assumed parameters are calculated to meet the ISO-14687 [30] standard of the product hydrogen. Notably, the information listed in Table 3 is an example data for the validation of the algorithm developed in this study. It is not the design of the SMR-PSA process for actual hydrogen production; therefore, no optimization has been performed.

Table 3. Process parameters of an example study

Feed composition	H_2 (%)	80	
	CO_2 (%)	20	
Adsorption pressure	bar	10	
Desorption pressure	bar	1	
Feed flow rate	SLPM	23	
Purge flow rate	SLPM	1	
Ambient temperature	°C	25	
Feed-gas inlet temperature	°C	40	
H_2 purity	%	99.97	
H_2 recovery	%	63.11	
t1	s	120	*See Fig. 3
t2	s	120	

Under the conditions mentioned in Table 3, the PSA plant is expected to produce 99.97% pure hydrogen with 63.11% recovery after the dynamic equilibrium state. The dataset used for training includes temperature data, which comprise some of the most reliable information that can be obtained from a PSA plant. The temperature is measured at the center of the adsorption column and

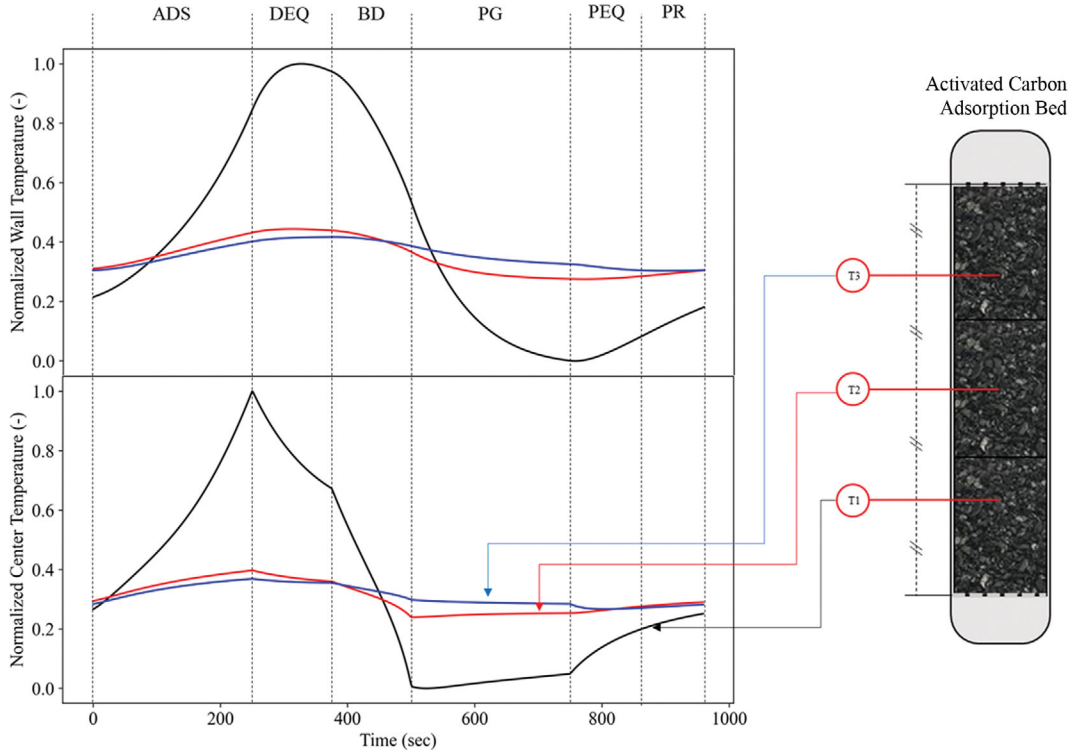

Fig. 5. Wall and bed-center temperature profiles for a single bed.

the wall. The measurement locations of temperature profiles are assumed to be at 1/4, 2/4, and 3/4 of the column (25, 50, and 75 cm). Fig. 5 shows the wall and bed-center temperature profiles for a single bed after dynamic equilibrium is reached. Fig. 5 shows the process of desorption (DEQ, BD, and PG) losing heat and adsorption (PEQ, ADS, and PR) gaining heat. The exothermic and endothermic effects of adsorption increase with increasing adsorption and desorption. Therefore, in theory, if the pattern can be learned well, the adsorption performance of the internal adsorbent can be predicted using the temperature evolution profile.

A dataset for supervised learning is generated by determining 1000 cases with a randomly generated adsorbent degradation factor k_d. Our study does not consider changing other factors such as the time sequence, ambient temperature, feed, and pure flow rate. The variation of k_d (see Eq. (6)) in the generated dataset ranges from 0.5 to 1.0. It is important to note that an adsorbent that has lost more than half its isothermal adsorption capacity is an extreme case and requires urgent replacement. The measurement-location temperature data are min-max normalized. The input data for the most extreme degradation case (k_d=0.5) and the case where no degradation occurred (k_d=1) are shown in Figs. 6 and 7.

As the adsorption capacity decreases due to the adsorbent degradation, the amount of adsorption also decreases. Therefore, adsorption heat generation might also be decreased. However, the overall temperature profile will change as the residual CO_2 that is not sufficiently removed is transferred to the adsorbent in a higher position. Because the PSA system is a dynamic process that involves a combination of adsorption and desorption, as shown in Figs. 6 and 7, these trends are not monotonic. The wall and center temperatures of the adsorption tower exhibit a similar trend, although the wall temperature tends to be broader due to the relatively high thermal inertia. The next section explains how deep learning algorithms can be used to infer the degree of degradation from these time-series data.

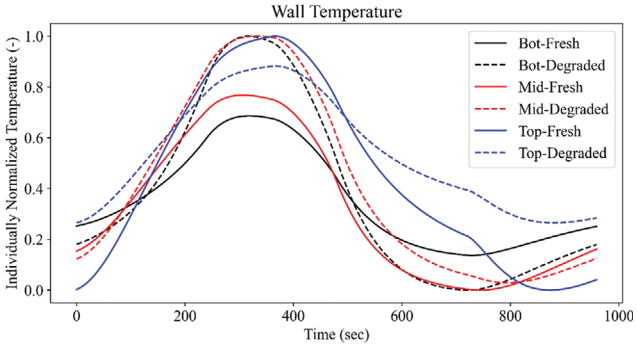

Fig. 6. Normalized wall-temperature data for degraded (k_d=0.5) and fresh (k_d=1) conditions.

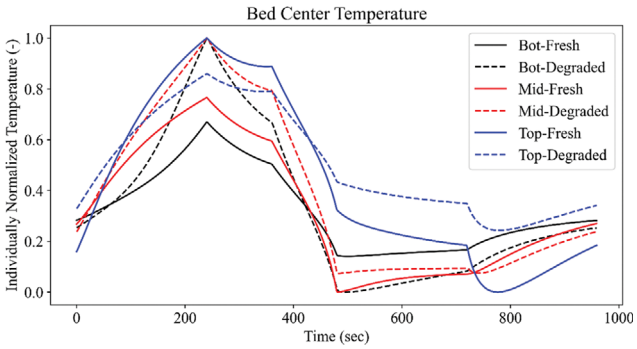

Fig. 7. Normalized bed-center temperature data for degraded (k_d=0.5) and fresh (k_d=1) conditions.

DEEP LEARNING MODEL

This study proposes a method for developing a diagnosis methodology for adsorbents inside the PSA. The method involves using a pretrained neural network that is supervised based on the performance-degraded PSA's time-series database generated through the simulator. Several algorithms exist to regress degree from such time-series information; this study proposes applying the Conv1D-long-short-term memory (LSTM) or Conv1D-LMST model [31].

1. Conv1D-LSTM Model Structure

Zhang et al. reported that the Conv1D-LSTM model performs better than other algorithms in predicting the performance degradation of the wind-turbine front bearing using multiple time-series data [28], which is a task that is similar to the one in this research. The proposed algorithm combines two well-known time-series-data-processing models, namely the 1D convolutional neural network (1D CNN) [32] and long-short term memory (LSTM) [32].

One-dimensional convolutional neural networks (1D-CNN) are a specific type of neural network architecture primarily used for extracting features from fixed-length segments of sequences, such as time-series data. Unlike feedforward or recurrent neural networks, 1D-CNNs apply convolutional filters along a single spatial (or temporal) dimension in the input data, making them particularly effective for analyzing temporal dependencies and local patterns within the data. The primary components of a 1D-CNN are convolutional layers, each of which uses a set of learnable filters or kernels. Each kernel in the layer is convolved across the time sequence to produce a feature map. This operation involves the element-wise multiplication of the kernel with the input data, followed by a sum of the results. The 1D CNN is first used to extract features from the time-series data, and then the extracted features are trained back into the time-series model using LSTM, which is a type of recurrent neural network (RNN) architecture, utilized in the field of deep learning. Unlike traditional feedforward neural networks, feedback connections are included in LSTM. It can process not only single data points, but entire sequences of data. Applications such as speech recognition, language modeling, and translation have seen successful usage of these networks. Memory cells, the defining feature of an LSTM network, are designed to store and recall information over long periods of time. They prevent issues related to vanishing and exploding gradients that standard RNNs often encounter. The control over this memory is exerted through structures called gates. LSTMs are typically utilized for sequence-to-sequence prediction, but sequence-to-value regression is also possible by connecting the output vector of the last stage of the LSTM with a feed forward network for supervised learning. In this study, a supervised learning methodology was applied to regress k_d from sequence temperature profile input.

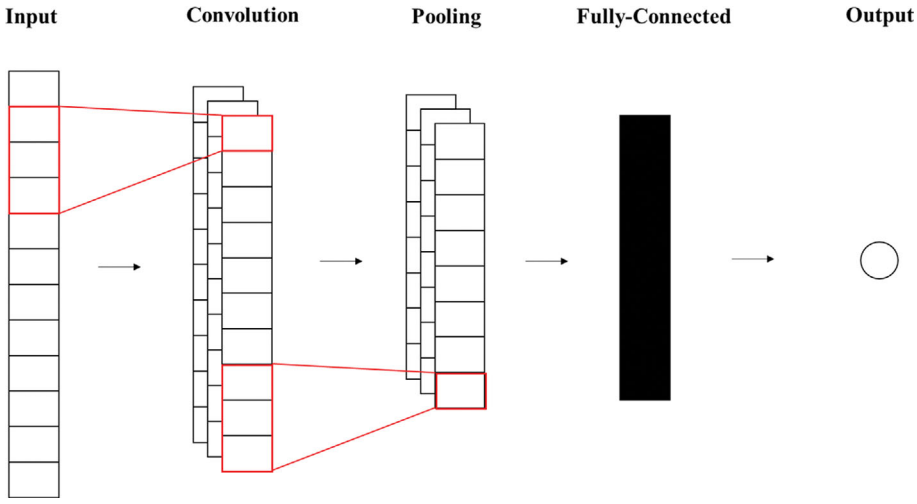

Fig. 8. Network structure of a 1D CNN.

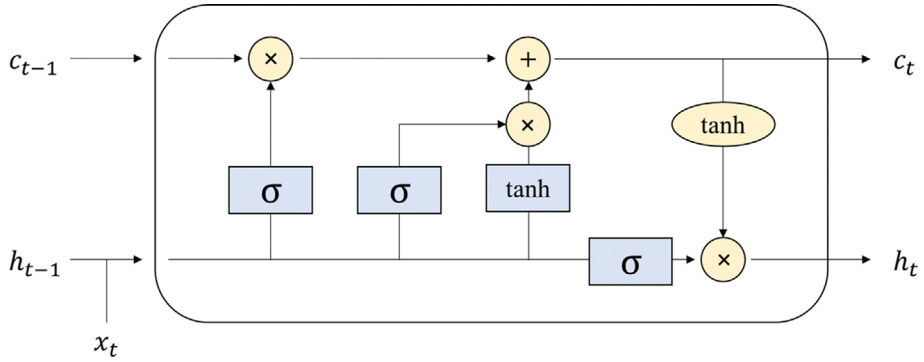

Fig. 9. Network structure of LSTM.

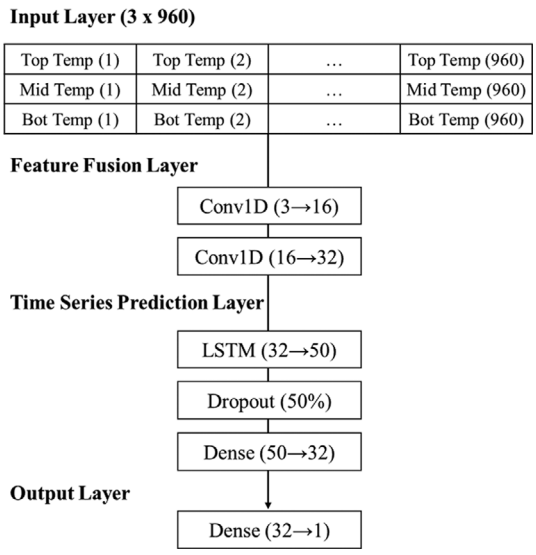

Fig. 10. Network structure and hyperparameters of the Conv1D-LSTM model.

The structure of a 1D CNN is shown in Fig. 8, whereas the network structure of an LSTM is shown in Fig. 9. Fig. 10 shows the structure and hyperparameters of the Conv1D-LSTM model used in this study. For the Conv1D layer, kernel size=3, stride=1, and padding=1. An LSTM was used by declaring a structure with input size 32, hidden size 50, and containing only one hidden layer.

2. Training the Conv1D-LSTM Network

A database for machine learning is developed using the given materials to create the diagnosis algorithm. The performance of the internal adsorbent is evaluated through information that can be acquired easily in real time while the PSA is in operation; therefore, time-series data of the adsorption-bed-center temperature and wall temperature are selected as the input. The accessibility, difficulty of measurement, and response speed of the measuring sensor are taken into consideration when selecting these parameters. It is assumed that temperature data are measured at three locations, that is, the top, middle, and bottom of the adsorption bed, considering the monitoring system operating in a typical PSA. The performance of the model is evaluated using mean absolute error (MAE), mean absolute percentage error (MAPE), and root mean squared error (RMSE) as metrics. Eq. (8) provides the definition of each error.

Metrics to evaluate the performance of the Conv1D-LSTM model:

$$\mathrm{MAE}=\frac{1}{n}\Sigma|e_t| \quad \mathrm{MAPE}=\frac{1}{n}\Sigma\frac{|e_t|}{d_t} \quad \mathrm{RMSE}=\sqrt{\frac{1}{n}\Sigma e_t^2}, \tag{8}$$

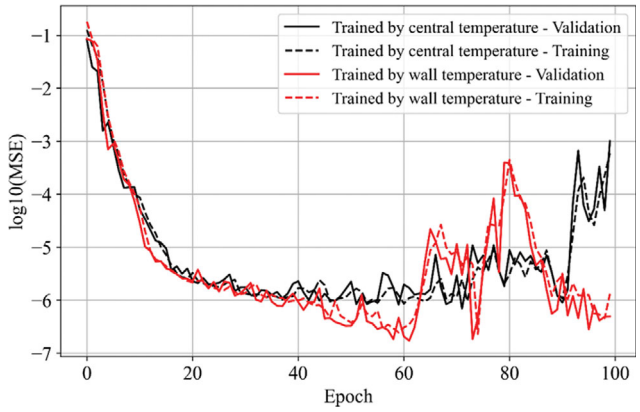

Fig. 11. Training and validation loss through epochs.

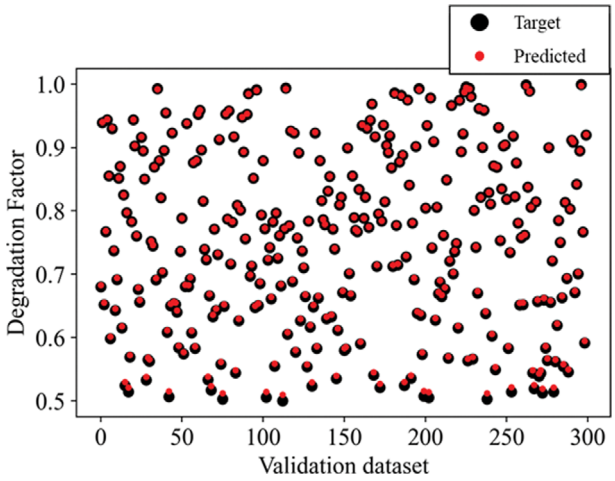

Fig. 12. Visualization of the predicted adsorbent-degradation factor k_d and the target.

where e_t is error, n is the number of samples, and d_t is the actual value.

Notably, network training progressed with Pytorch 1.13.1 [34] in the Python 3.7 environment [25]. Of the total 1000 datasets, 70% were used for training and 30% for validation.

RESULTS

Fig. 11 shows the training and validation loss through epochs when using either the wall or the bed-center temperature profiles as input for the training. The Conv1D-LSTM model shows that training and validation losses reached high accuracy, with an order of 10^{-6} for both datasets.

The results in Fig. 11 demonstrate that the proposed model can achieve a satisfactory level of MSE loss (10^{-6} order) regardless of whether the wall or the bed-center temperature profile is used. These findings suggest that the proposed methodology can successfully work with either temperature data profile and that the selection of the sensor installation location should be based on the device's

Table 4. Performance metrics of pretrained network

Trained by the wall temperature			Trained by the bed-center temperature		
MAE	MAPE	RMSE	MAE	MAPE	RMSE
5.57E-04	6.47E-03	6.82E-04	1.36E-03	2.27E-02	1.80E-03

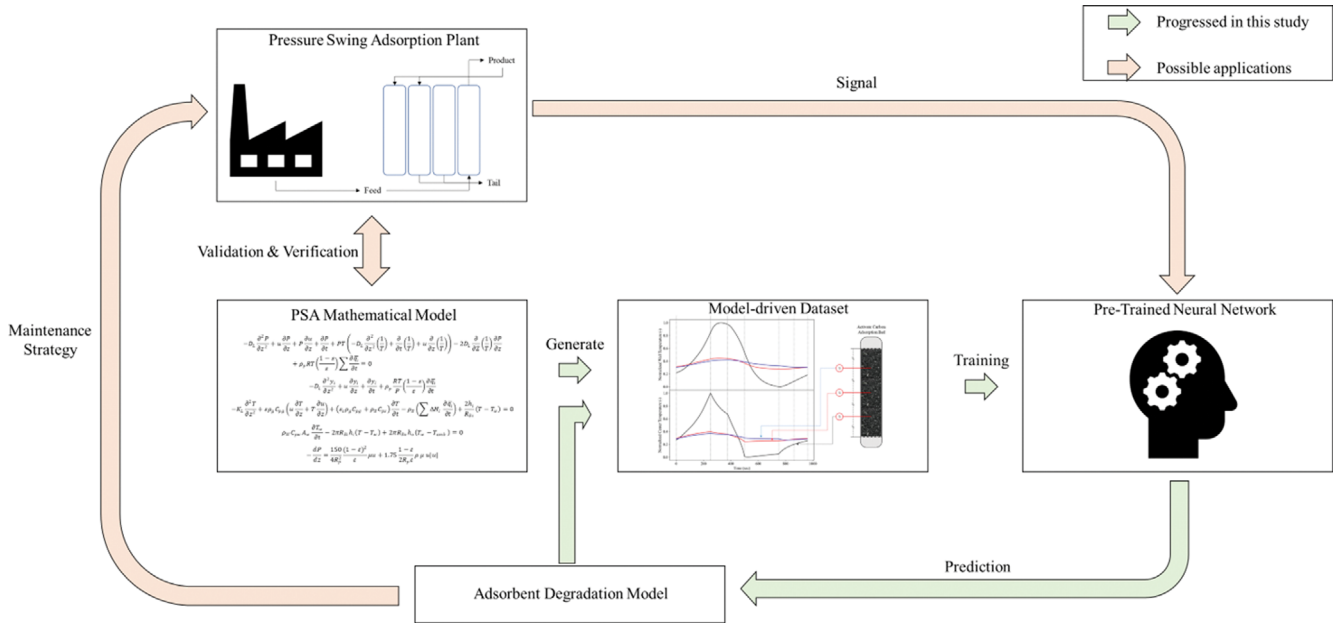

Fig. 13. Summary of progressed research and possible applications.

installation environment. However, the results show that if external problems can be handled, the pretrained network via the wall-temperature profile has higher prediction performance compared to the pretrained network via the bed-center temperature profile.

Table 4 shows the metrics of the pretrained network at the optimum point where the MSE loss is the smallest. Furthermore, Fig. 12 shows the visualization of the predicted adsorbent-degradation factor k_d and the target. As shown in Table 4 and Fig. 12, the developed diagnosis algorithm can successfully predict the performance degradation of the adsorbents.

Fig. 13 shows a graphical summary of the developed methodology. The performance degradation learning technique based on the simulator developed in this study presents a methodology that can predict the gradual performance degradation of the adsorbent in real-time during the long-cycle PSA operation in cyclic quasi steady state. This technique is expected to enable future cycle optimization or maintenance strategy formulation commensurate with the degree of adsorbent performance degradation.

CONCLUSIONS AND DISCUSSION

This study presents a methodology for diagnosing the performance deterioration of the adsorbent loaded in a PSA plant based on externally measured information without stopping the operation of the plant. First, a well-fitted 1D PSA simulator was developed, and a database was generated by applying the performance degradation model of the adsorbent to the simulator. Then, the behavior change of the PSA plant according to the deterioration of the adsorbent was trained using the Conv1D-LSTM network through the database. Finally, the performance deterioration of the adsorbent loaded into the PSA plant was diagnosed through the pretrained neural network.

This study confirms that the performance deterioration of the adsorbent can be predicted with an MSE of 10^{-6} through the developed diagnosis algorithm using SMR-PSA as an example. By applying the developed methodology, I can establish an adsorbent replacement cycle and a predictive maintenance strategy by identifying the degree of PSA performance deterioration in real time. Additionally, the optimization of the PSA operation timetable can be considered for more efficient operation, while reducing operation and maintenance costs. While this study predominantly employs a Conv1D-LSTM network, similar methodologies could potentially be applied to other time series networks. Examples include the recurrent neural network (RNN), gated recurrent unit (GRU), transformer, among others.

However, additional research and development is required because this research is still in the proposal stage and experimental verification has not yet been conducted in real industrial settings. The study has the following limitations.

1. A study of the deterioration mechanism of adsorbents and the isotherm curve and mass transfer coefficient change of the adsorbents degraded individually is necessary for applying the PSA plant.
2. More variables will change in the actual field, such as seasonal changes in ambient temperature, the pressure at the top of the adsorption bed, and the feed-gas composition. Therefore, diagnosis algorithms that enable performance prediction even while considering these changes are necessary.
3. This study is about developing an algorithm for determining the degree of deterioration. Additional studies, such as replacement-cycle determination and cycle optimization considering the degree of deterioration, need to be conducted.
4. This study assumes that all adsorption beds have degraded to the same extent, so further research is needed to determine if a specific bed has degraded excessively. For example, it can happen due to abnormal situations, such as rapid performance degradation due to the inhalation of impurities or incidents. Further researches are required for these types of situations.
5. This study assumed that the degree of porosity and adsorbent degradation would be equalized within the bed after degradation, but in reality, more severe degradation may occur at the bottom site where the feed gas enters. This unbalanced degradation distribution needs further study.

Despite these limitations, the proposed methodology presents the possibility of quantitatively diagnosing the degree of deterioration of the adsorbent in a PSA, which has not been easily measured so far with high accuracy. Compared to the traditional stop-and-sample methodology, the methodology herein is expected to have a higher potential for real-world industrial applications, because it enables real-time diagnosis through time series information of temperature that is easy to measure and accessible in real time. This research can be applied especially in PSA processes performed on feed gas that includes impurities that inevitably cause damage to the adsorbent, such as by-product hydrogen production, CO_2 capture with exhaust gas, and ammonia cracking.

ACKNOWLEDGEMENT

This study was conducted with the support of the Kyungpook National University and Research Insititute of Industrial Science and Technology (RIST) individual project.

NOMENCLATURE

Latin Letters

A_w : wall cross-sectional area [m^2]
C : diffusion time constant [sec^{-1}]
C_{pg}, C_{ps}, C_{pw} : heat capacity of gas, pellet and wall [J/kg K]
D_L : axial dispersion coefficient [m^2/s]
h_i : internal heat transfer coefficient [J/m^2 K s]
h_o : external heat transfer coefficient [J/m^2 K s]
ΔH : heat of adsorption [J/mol]
K_L : axial thermal conductivity [J/m K s]
k_d : adsorbent degradation factor [-]
L : bed length [m]
P : total pressure [Pa]
q, q^*, $\bar{q}$: adsorption loading amount, adsorption isotherm, average concentration [mmol/g]
R : gas constant [8.31447 J/mol K]
R_P : pellet radius [m]
R_{Bi} : bed inner radius [m]
R_{Bo} : bed outer radius [m]

t : time [sec]
T_{amb} : ambient temperature [K]
T : bed temperature [K]
T_w : wall temperature [K]
u : interstitial velocity [m/s]
y_i : mole fraction of species *i* in gas phase [-]
z : axial distance in bed from the feed gas inlet [m]

Abbreviations

ADS : adsorption step
BD : blowdown step
DEQ : depressurizing pressure equalization step
PEQ : pressurizing pressure equalization step
PR : pressurization step
PG : purge step
LSTM : long-short term memory

Greek Letters

α : particle porosity [-]
ε : voidage of adsorbent bed [-]
ε_t : total void fraction [-]
μ : viscosity [Pa sec]
ρ_g, ρ_p, ρ_B, ρ_w : density of gas, pellet, bulk and bed wall [kg/m^3]
ω : linear driving force (LDF) coefficient [sec^{-1}]

REFERENCES

1. L. T. Biegler, L. Jiang and V. G. Fox, *Sep. Purif. Rev.*, **33**(1), 1 (2005).
2. D. W. Siderius, V. K. Shen, R. D., III Johnson and R. D. van Zee, NIST/ARPA-E Database of Novel and Emerging Adsorbent Materials, NIST Standard Reference Database Number 205; National Institute of Standards and Technology: Gaithersburg, MD, http://adsorbents.nist.gov (retrieved July 07, 2023).
3. C. W. Wu and S. Sircar, *Adsorption*, **25**, 669 (2019).
4. M. Luberti and H. Ahn, *Int. J. Hydrogen Energy*, **47**(20), 10911 (2022).
5. A. D. Wiheeb, Z. Helwani, J. Kim and M. R. Othman, *Sep. Purif. Rev.*, **45**(2), 108 (2016).
6. M. D. Sees, T. Kirkes and C. C. Chen, *Comput. Chem. Eng.*, **147**, 107235 (2021).
7. M. A. Makarem, M. Mofarahi, B. Jafarian and C. H. Lee, *Comput. Chem. Eng.*, **121**, 483 (2019).
8. J. Uebbing, L. T. Biegler, L. Rihko-Struckmann, S. Sager and K. Sundmacher, *Comput. Chem. Eng.*, **151**, 107340 (2021).
9. R. Rajasree and A. S. Moharir, *Comput. Chem. Eng.*, **24**(11), 2493 (2000).
10. A. Streb and M. Mazzotti, *Comput. Chem. Eng.*, **166**, 107974 (2022).
11. F. G. Wiessner, *Gas Sep. Purif.*, **2**(3), 115 (1988).
12. C. J. Heard, L. Grajciar, F. Uhlík, M. Shamzhy, M. Opanasenko, J. Čejka and P. Nachtigall, *Adv. Mater.*, **32**(44), 2003264 (2020).
13. R. Razzaq, C. Li and S. Zhang, *Fuel*, **113**, 287 (2013).
14. H. Ahn, J. Yang and C. H. Lee, *Adsorption*, **7**, 339 (2001).
15. K. O. Iwuozor, J. O. Ighalo, E. C. Emenike, L. A. Ogunfowora and C. A. Igwegbe, *Curr. Res. Green Sust. Chem.*, **4**, 100179 (2021).
16. S. Kulkarni and J. Kaware, *Int. J. Innov. Sci. Eng. Technol.*, **1**(8), 61 (2014).
17. J. G. Jee, M. B. Kim and C. H. Lee, *Chem. Eng. Sci.*, **60**(3), 869 (2005).
18. C. H. Lee, J. Yang and H. Ahn, *AIChE J.*, **45**(3), 535 (1999).
19. J. P. Mota and A. J. Rodrigo, *Ind. Eng. Chem. Res.*, **39**(7), 2459 (2000).
20. J. H. Yun, D. K. Choi and H. Moon, *Chem. Eng. Sci.*, **55**(23), 5857 (2000).
21. M. B. Kim, J. H. Moon, C. H. Lee, H. Ahn and W. Cho, *Korean J. Chem. Eng.*, **21**, 703 (2004).
20. I. F. Macdonald, M. S. El-Sayed, K. Mow and F. A. L. Dullien, *Ind. Eng. Chem. Fundam.*, **18**(3), 199 (1979).
21. N. S. Raghavan, M. M. Hassan and D. M. Ruthven, *Chem. Eng. Sci.*, **41**(11), 2787 (1986).
22. C. T. Choi and H. Wen-Chung, *Chem. Eng. Sci.*, **49**(1), 75 (1994).
23. L. Guo, W. A. Jury, R. J. Wagenet and M. Flury, *J. Contam. Hydrol.*, **43**(1), 45 (2000).
24. T. Paszko and M. Jankowska, *Ecotox. Environ. Safe.*, **161**, 584 (2018).
25. G. Van Rossum and F. L. Drake, *Python 3 reference manual*, Scotts Valley, CA: CreateSpace (2009).
26. H. Ahn, C. Chun, M. Park, I. S. Ahn and C. H. Lee, *Sep. Sci. Technol.*, **36**(10), 2121 (2001).
27. S. Ahn, Y. W. You, D. G. Lee, K. H. Kim, M. Oh and C. H. Lee, *Chem. Eng. Sci.*, **68**(1), 413 (2012).
28. L. Barelli, G. Bidini, F. Gallorini and S. Servili, *Energy*, **33**(4), 554 (2008).
29. L. Riboldi and O. Bolland, *Energy Procedia*, **114**, 2390 (2017).
30. ISO/TC 197 (2019). Hydrogen Technologies. ISO 14687 Hydrogen Fuel—Product Specification—Part 2: Proton Exchange Membrane (PEM) Fuel Cell Applications for Road Vehicles. Available online: https://www.iso.org/obp/ui/fr/#iso:std:iso.14687-1:v1:en (retrieved July 07, 2023).
31. S. Zhang, T. Zhang and Y. Liu, International Conference on Industrial Engineering and Engineering Management (IEEM), 1029 (2021).
32. S. Kiranyaz, O. Avci, O. Abdeljaber, T. Ince, M. Gabbouj and D. J. Inman, *Mech. Syst. Signal Proc.*, **151**, 107398 (2021).
33. Y. Yu, X. Si, C. Hu and J. Zhang, *Neural Comput.*, **31**(7), 1235 (2019).
34. A. Paszke, S. Gross, F. Massa, A. Lerer, J. Bradbury, G. Chanan, T. Killeen, Z. Lin, N. Gimelshein, L. Antiga, A. Desmaison, A. Kopf, E. Yang, Z. DeVito, M. Raison, A. Tejani, S. Chilamkurthy, B. Steiner, L. Fang, J. Bai and S. Chintala, *Adv. Neural Inf. Process. Syst.*, **32**, 8024 (2019).